

Three-Dimensional Printing of Lignocellulose Structures: Improving Mechanical Properties and Shape Fidelity

Yangxiaoze Jiang, Muhammad Latif, and Jaehwan Kim*

Cite This: *ACS Omega* 2024, 9, 23442–23450

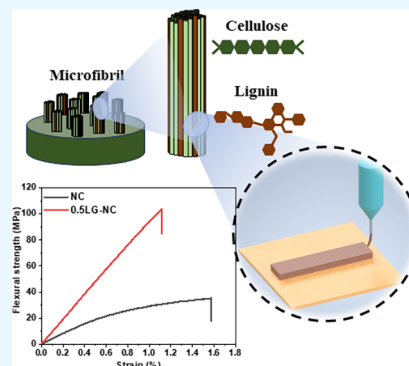
Read Online

ACCESS |

Metrics & More

Article Recommendations

ABSTRACT: Additive manufacturing of nanocellulose (NC) materials is an emergent technological domain that facilitates the fabrication of complex and environment-friendly structures that mitigate greenhouse gas emissions. However, printing high concentrations of NC into intricate structures encounters substantial challenges due to inadequate adhesion between the printed layers attributed to a high cellulose solid content, resulting in low shape fidelity and mechanical properties. Therefore, to address these challenges, this paper reports lignin (LG) blending, a nanofiller, in high-content NC (>25 wt % solid content) paste to improve the layer adhesion of three-dimensional (3D) printed structures. The printed structures are dried in a clean room condition followed by postcuring. The optimized lignocellulose (0.5LG-NC) paste showed high structural shape fidelity, remarkable flexural strength, and moduli of 102.93 ± 0.96 MPa and 9.05 ± 0.07 GPa. Furthermore, the volumetric shrinkage behavior in box-like 3D printed structures with optimized LG-NC paste shows low standard deviations, demonstrating the repeatability of the printed structures. The study can be adapted for high-performance engineering and biomedical applications to manufacture high mechanical strength environment-friendly structures.



1. INTRODUCTION

Three-dimensional (3D) printing, or additive manufacturing (AM) technology, creates physical objects from 3D models, usually layer-upon-layer patterns.¹ This technology can quickly fabricate micro-to-macro-scale freestanding 3D structures without mold using single or multiple materials.^{2,3} Depending on the materials, various AM techniques can be selected for fabricating 3D structures, including fused deposition molding (FDM), extrusion printing (EP), inkjet bioprinting, and powder fusion printing.^{4–7} FDM and EP are the most attractive for printing thermoplastic, thermoset, and biopolymer composites among different AM techniques. In FDM, thermoplastic filaments of polycarbonates, polylactic acid, and acrylonitrile butadiene styrene melt at the nozzle into a semiliquid state and are extruded in a layerwise pattern to fabricate 3D structures.^{8,9} In contrast, EP techniques can print precisely various materials, including thermosets and highly viscous wood-derived polymers such as nanocellulose under ambient conditions in a layerwise pattern.¹⁰

Due to the current climate change, people pay attention to using environmentally friendly materials that mitigate greenhouse gas (GHG) emissions. Wood-derived polymers have been getting much consideration for structural, energy storage devices and biomedical and electronic applications due to their environment-friendly behavior, abundance, and multifunctional properties.^{11–14} The natural components of wood include lignin, cellulose, and hemicelluloses, which form a hierarchical structure. These primary wood components are

accessible in large quantities in the industrial sector for various engineering applications.¹⁵ In the pulping process, lignin is deemed a waste component, but due to technological advancements, it is considered a viable choice as a stiff filler used in 3D printing for biomaterials and composites as a reinforcement.¹⁶ Hemicellulose links cellulose fibers into microfibrils with lignin to offer a high mechanical strength in plants. Cellulose, a green, sustainable, and renewable copious biopolymer on earth, is made up of repeated β -D-glucopyranose units covalently bonded by acetal functionalities between hydroxyl groups of C4 and C1 carbon atoms, offering its high-performance features.^{17,18} The microfibril and crystalline regions in cellulose are called cellulose nanofibers (CNF) and cellulose nanocrystals (CNC). CNC and CNF are combined, known as nanocellulose.¹⁹ Therefore, nanocellulose materials have been the subject of extensive research as a feedstock for 3D printing environmentally friendly materials due to their mitigating GHG emission benefits and unique characteristics, including high mechanical strength, optical transparency, and low thermal expansion.

Received: January 9, 2024

Revised: March 19, 2024

Accepted: March 22, 2024

Published: May 1, 2024



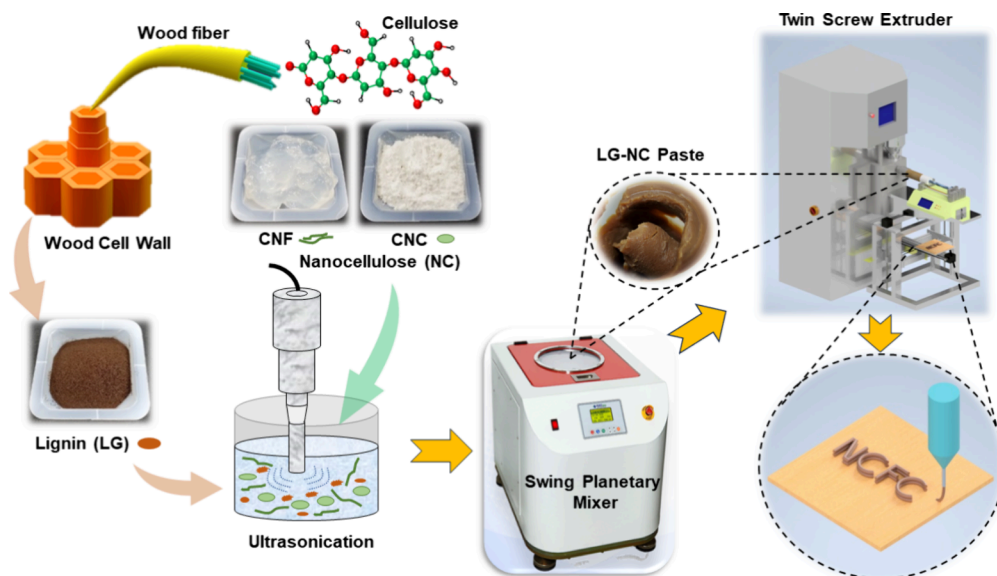


Figure 1. Schematic of the 3D printing process of LG-NC structures.

In recent years, low viscous suspensions of CNC (6.6 vol % relative to water) and CNF (1.3–2.6 vol % relative to water) have already been demonstrated for 3D printing employing extrusion-based AM for different applications.^{20–23} The main challenges in printing low-concentration nanocellulose structures include collapsing and shape fidelity or retention during printing and drying, related to the low solid content of nanocellulose.²⁴ However, the printed structures with a relatively high solid NC content of 25 wt % faced challenging issues, including bilayer adhesion, cracking between layers due to shrinkage, shape fidelity, protruding during drying, and repeatability.^{25–28} These 3D printed environmentally friendly structures do not have enough mechanical properties as exhibited in their bioresources. Thus, some efforts have been made to resolve these issues. Klar et al.²⁹ printed enzymatically treated NC of a 25 wt % solid content to improve the adhesion between printed layers under different drying conditions. The results suggested that the bilayer adhesion was insufficient to achieve high-performance NC structures, even after enzymatic treatment. Hausmann et al.³⁰ performed a wet densification process on 3D printed NC structures using organic and inorganic chemicals. After the wet densification process, the mechanical strength in the printed structures was improved but still not significant. Furthermore, the densification process is not suitable for large structures. In brief, the studies presented above proved that the concentrated NC structures could not achieve high mechanical strength, repeatability, and high shape fidelity without solving bilayer adhesion issues.

In this work, alkali-treated lignin was blended with the concentrated NC (25.45 wt %) paste, which was then 3D printed to obtain LG-NC structures. The schematic of the 3D printing process is shown in Figure 1. The prepared lignocellulose (LG-NC) paste is ejected through a twin-screw extrusion machine for 3D printing. In comparison, the pristine NC structures are also 3D printed. The 3D printed structures are dried at a relative humidity of 45% and a constant temperature of 25 °C. The main objectives of this work are to achieve mechanically strong and environmentally friendly 3D printed LG-NC structures and to investigate the role of LG in terms of layer adhesion, mechanical strength, and shape fidelity of the 3D printed structures. This is the first

attempt to explore the LG content effect as a nanofiller on adhesion between 3D printed layers, shape fidelity, and mechanical strength of the 3D printed LG-NC structures.

2. EXPERIMENTAL SECTION

2.1. Materials. The alkali-treated LG powder of a low sulfonate content was purchased from Sigma-Aldrich, South Korea. The CNC powder was obtained from CelluForce NCC, Canada. The TEMPO-oxidized CNF suspension (~2.05 wt % relative to water) was purchased from Moorim, South Korea. The bleached kraft pulp from hardwood was used for the CNF isolation, consisting of 79% cellulose, 19% hemicellulose, and small amounts of lignin and ash. The average diameter and length of CNF are 3.5 nm and 0.55 μm , respectively.

2.2. Preparation of Lignocellulose Paste. The pure high-content NC paste of the 25.45 wt % solid content was made by mixing CNF with CNC in a ratio of 20:1 (CNC:CNF) using a swing planetary mixer (SPM, FDU-2200, Tokyo Rikakikai Co., Japan) for 10 min at 1200 rpm. Furthermore, the LG powder was well homogenized in deionized (DI) water using a digital ultrasonic homogenizer (SONOPLUS HD 2070.2 SET, Bandelin, Germany) for 10 min before mixing with the NC paste as a cross-linker. The different contents of the homogenized LG filler (CNF:CNC:LG = 20:1:0.25, 0.5, and 0.75) were mixed in the NC using the SPM for 15 min at 1200 rpm. The composition of all prepared pastes is shown in Table 1. The prepared LG-NC pastes were named x LG-NC depending on the LG content, x . They were stored in the fridge before 3D printing.

Table 1. Composition of All Prepared LG-NC Pastes

paste composition	CNC (g)	CNF (g)	LG (g)	total solid content (g)
CNC-CNF	24.25	1.20	0	25.45
CNC-CNF-0.25LG	24.25	1.20	0.3	25.75
CNC-CNF-0.5LG	24.25	1.20	0.6	26.05
CNC-CNF-0.75LG	24.25	1.20	0.9	26.35

2.3. 3D Printing Setup. The whole 3D printing process is shown in Figure 1. The prepared high LG-NC paste was injected into the twin-screw extruder (MC 15 HT, Xplore, The Netherlands) using a high-precision syringe pump (Nexus 6000, Chemyx, USA) operating at a controlled feed rate of 1.2 mL/min. The exit of the twin-screw extruder was directly linked to a 3D printing stage, which was further connected with a 1.51 mm diameter nozzle fixed to the printing stage for executing the 3D printing process. The rotational speed of the twin-screw extruder was optimized at 150 rpm to align with a desired printing speed of 9.37 mm/s. The commercially accessible software “Cura” was employed to convert computer-aided design (CAD) files into g-code files. The printing parameters (screw speed, feeding rate, and printing speed) were optimized for high-content LG-NC paste to ensure extrudability and freestanding wet structures in a layerwise pattern.

2.4. Drying Conditions. The drying conditions of the 3D printed LG-NC structures are responsible for the adhesion issues between the printed layers, resulting in low shape fidelity/retention. Thus, the 3D printed LG-NC structures were subjected to a 5 day drying period in a controlled clean room environment at a consistent relative humidity (RH) of 45% and a temperature of 25 °C, ensuring effective moisture removal. Following this initial drying phase, the structures were subjected to postcuring in a vacuum oven at 140 °C for 30 min. This postcuring step will further enhance the structures' structural and material characteristics. Optimal drying conditions are crucial for achieving high shape fidelity in NC structures after water evaporation, which results in volumetric shrinkage. The 3D printed NC structures show poor shape fidelity due to adhesion issues between the printed layers during ambient and highly humid drying conditions.²⁸ Therefore, we chose clean room conditions for drying to improve the adhesion between the layers by optimizing the lignin content in the NC paste.

2.5. Characterizations. According to ASTM D790-03, the bending test was carried out on the 3D printed rectangular shape specimens using a universal testing machine (TO-100-IC, TEST ONE, South Korea) equipped with a 10 kN load cell. After the bending test, the cross section and surface of broken samples were observed using SEM (S4000, Hitachi, Japan) after platinum coating with a sputtering machine (KS75X, EMITECH, England). Furthermore, Fourier transform infrared (FTIR) (Cary 630, Agilent Technologies, USA) verified the cross-linking between NC and LG in the 3D printed LG-NC structures.

The optimized LG-NC paste (0.5LG-NC) was used to print 16 box-shaped structures with dimensions of 12.08 × 12.08 × 9.31 mm³ to ensure repeatability and shape fidelity. Moreover, the optimized lignocellulose paste formulation was employed in fabricating intricate LG-NC structures, i.e., scaffolds and flower vases, thereby affirming the adaptability and versatility of the LG-NC paste for diverse structural applications. The dimensions of the box-shaped structures were carefully measured using a digital micrometer (Mitutoyo 293-801, Japan).

3. RESULTS AND DISCUSSION

3.1. Paste Printability and Drying. The primary goal of this research is to increase the NC solid content and mechanical strength in 3D printed structures while avoiding concerns with printability, layer adhesion, and shape integrity.

Therefore, we prepared a high solid content LG-NC paste containing different LG contents and extruded it through a twin-screw extrusion machine at room temperature, ensuring the printability factor. The rheological properties of nanocellulose paste determine the printability factor for making 3D structures.³¹ Low-content NC reveals shear thinning behavior, allowing the printing of freestanding 3D structures. However, the printability for high-concentration NC using a twin-screw extruder depends on the continuous and homogeneous flow of the paste without clogging and freestanding of wet structures in a layerwise pattern. Therefore, the printing parameters of the twin-screw extrusion machine were properly optimized, including the feeding rate (mL/min), extrusion speed (mL/s), twin-screw speed (rpm), and flow rate (mL/min). After the printing parameters were optimized, the LG-NC paste was 3D printed on a wood substrate. The wet samples were kept in a clean room condition (45 RH% and 25 °C) for 5 days before being postcured in a vacuum oven. Figure 2 shows photo-

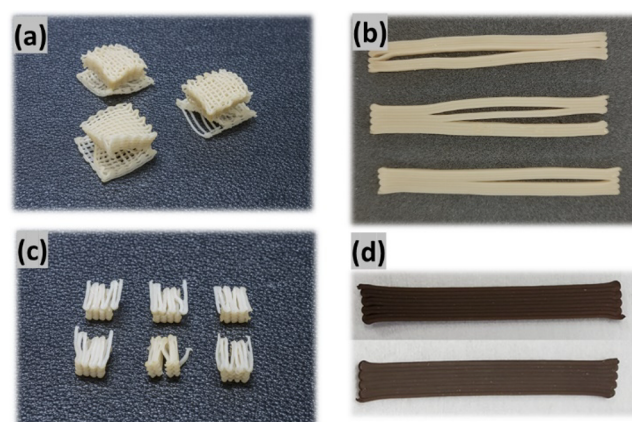


Figure 2. 3D printed and dried structures with (a–c) NC and (d) LG-NC paste.

graphs of the dried NC (a–c) and LG-NC (d) paste structures. The pure NC paste structure reflects low adhesion between the printed layers after drying because of the high solid content of NC. The NC structure shows a low shape fidelity after drying. However, the LG-NC structure shows a strong adhesion between the printed layers, representing no adhesion issues between printed layers, bulging, and cracking compared to those of the pure NC structure. The enhanced adhesion between the LG-NC printed layers may be associated with improved hydrogen bonding caused by the LG content in the NC paste. Furthermore, the 3D printed LG-NC structure exhibits a high shape fidelity without bilayer adhesion issues.

3.2. Chemical Interactions between LG and NC. The interactions between LG and NC functional groups are shown in Figure 3a. FTIR confirmed the interaction between the NC and LG after the postcuring, and the results are shown in Figure 3b. The LG-NC structure was made with a 0.5LG-NC paste. CNF and CNC exhibit characteristic bands at 1602 and 1647 cm⁻¹, respectively, which belong to the bending vibration of –OH groups. The FTIR spectrum of NC exhibits the absorption bands at 3390, 1642, and 1110 cm⁻¹, corresponding to the stretching of the hydroxyl group, bending vibration of –OH, and stretching vibration of –C–O, respectively.³¹ In the FTIR of NC, the band of CNC at 1647 cm⁻¹ shifted toward the slightly lower wavenumber at 1642 cm⁻¹, although the band of CNF at 1602 cm⁻¹ shifted toward the higher

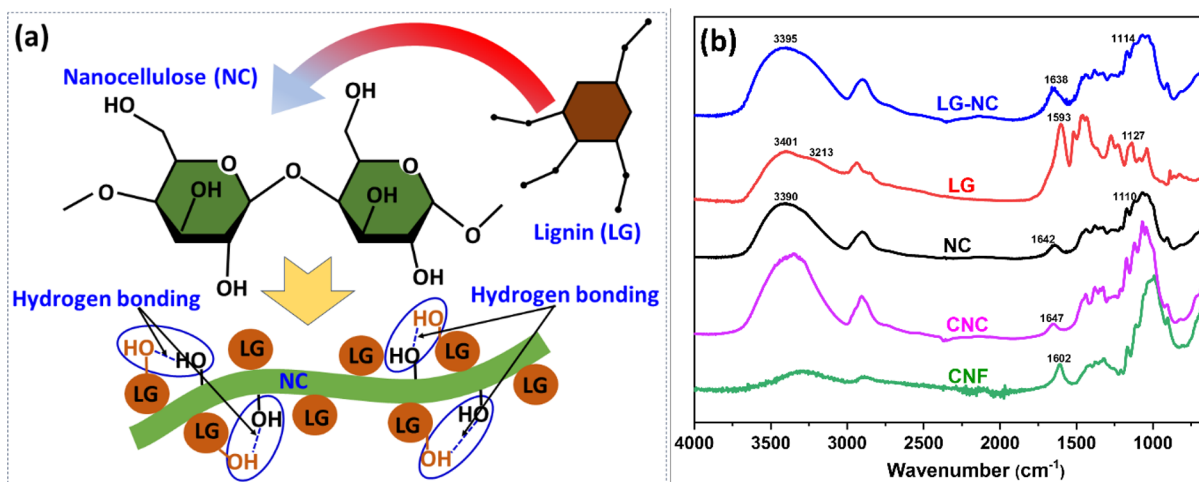


Figure 3. 3D printed lignocellulose: (a) chemical interactions and (b) FTIR spectra of NC, LG, and LG-NC structures.

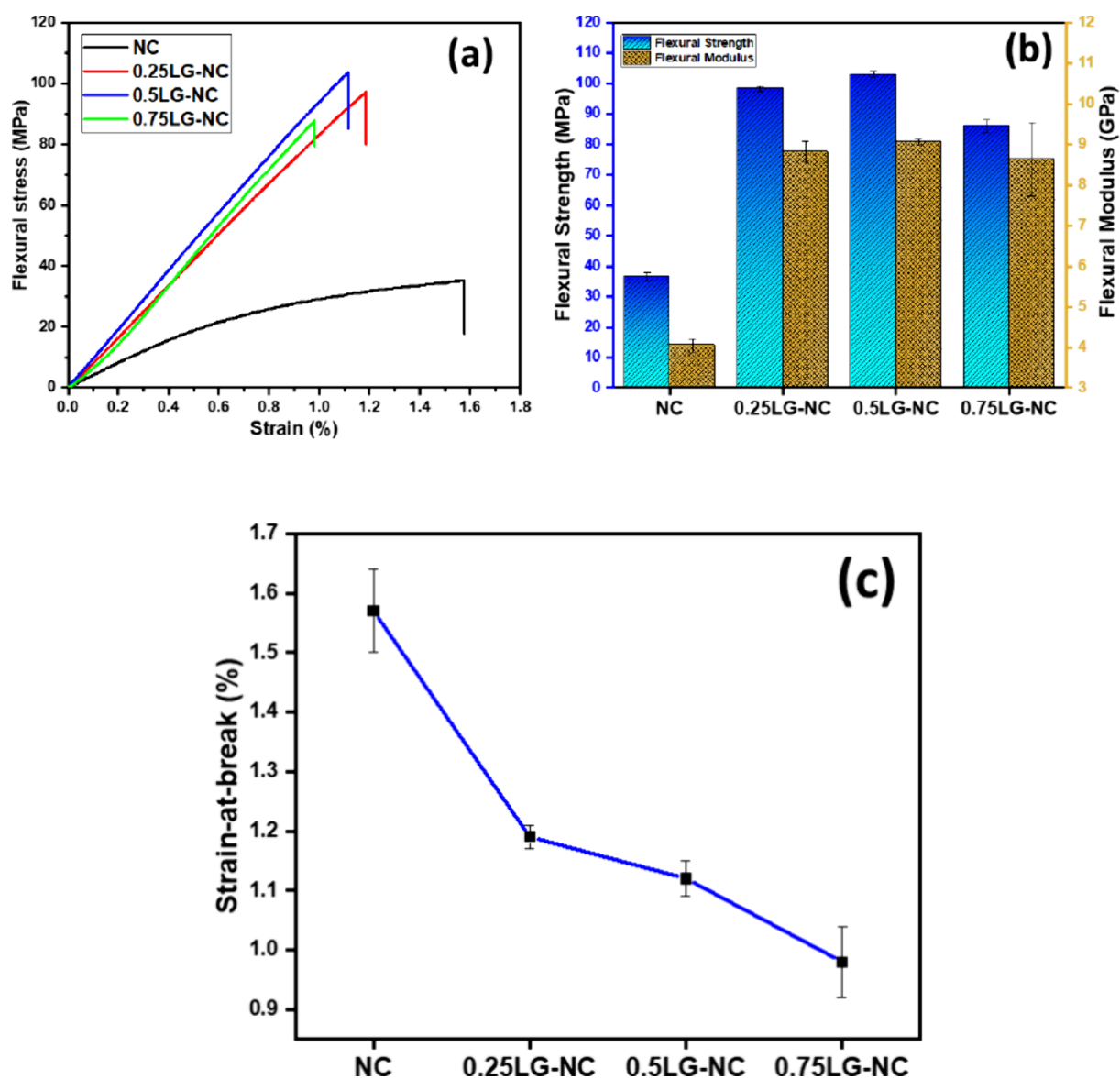


Figure 4. Mechanical properties of 3D printed LG-NC structures: (a) stress–strain curves, (b) bar graphs exhibiting flexural strength and modulus, and (c) strain-at-break.

Table 2. Mechanical Properties of 3D Printed Pure and Lignocellulose Structures

samples	solid content (wt %)	drying conditions	postcuring temperature (30 min)	flexural strength (MPa)	flexural modulus (GPa)	strain-at-break
NC	25.45	clean room		36.26 ± 1.45	4.04 ± 0.16	1.57 ± 0.07
0.25LG-NC	25.68	clean room	140 °C	98.23 ± 0.92	8.81 ± 0.26	1.19 ± 0.02
0.5LG-NC	25.90	clean room	140 °C	102.93 ± 0.96	9.05 ± 0.07	1.12 ± 0.03
0.75LG-NC	26.12	clean room	140 °C	85.98 ± 1.96	8.63 ± 1.01	0.98 ± 0.06

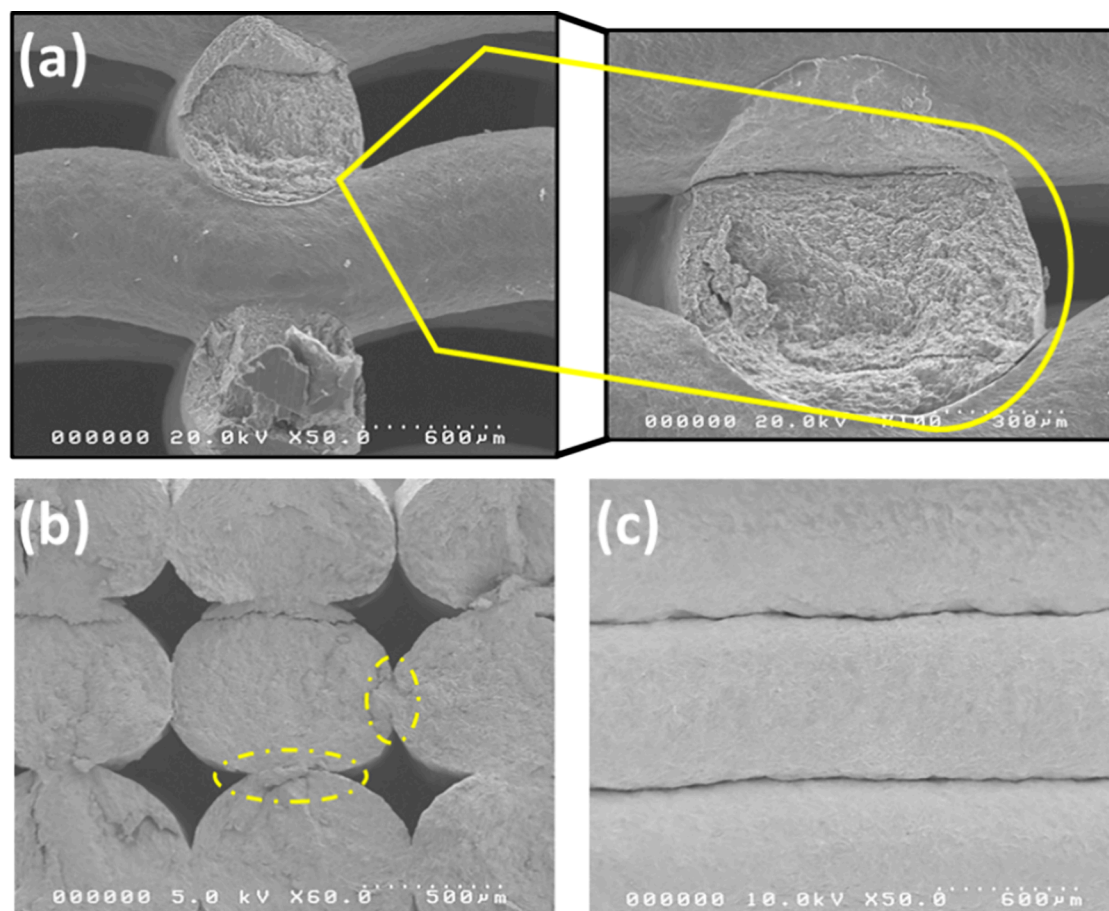


Figure 5. SEM images of the 3D printed 0.5LG-NC structure: (a) cross-sectional morphology of the scaffold, (b) cross-sectional morphology of the rectangular-shaped specimen, and (c) side view of the rectangular-shaped specimen.

wavenumber, which indicates the hydrogen bonding between the CNC and CNF. In the case of pure LG, the broadband in the $3200\text{--}3500\text{ cm}^{-1}$ region is due to the --OH stretching of aromatic and aliphatic. Peaks at 1593 and 1127 cm^{-1} are related to the aromatic skeleton vibrations and the --C--O ether group.³² However, after adding LG to the NC paste, the band intensity of LG-NC at 3395 cm^{-1} slightly increased.³³ Additionally, the aromatic hydroxyl band (3213 cm^{-1}) of LG merged due to hydrogen bonding between the --OH groups of LG and NC (Figure 3a). Moreover, the absorption band at 1642 cm^{-1} , corresponding to the --OH bending and --COO-- group in NC, shifted toward the slightly lower wavenumber at 1638 cm^{-1} due to hydrogen bonding between LG and NC.³⁴ These changes indicate the improved hydrogen bonding between the functional groups of NC and LG. The improved hydrogen bonding in the optimized 0.5LG-NC structure is responsible for strong interfacial adhesion between the printed layers, consequently improving the mechanical strength.

3.3. Mechanical Properties. Figure 4a–c shows the dependency of the mechanical strength behavior for the

pristine NC with increasing LG content. The stress–strain curves of all 3D printed LG-NC structures are shown in Figure 4a. Overall, the flexural strength, modulus, and strain-at-break of the pristine NC and LG-NC structures are represented in Table 2. As shown in Figure 4b,c, the average flexural strength, flexural modulus, and strain-at-break of the high-content (25.45 wt %) NC structure are 36.26 ± 1.45 MPa, 4.04 ± 0.16 GPa, and 1.57 ± 0.07 , respectively, reflecting low adhesions between the printed layers after drying.

All LG-NC structures show higher flexural strength and modulus, reflecting improved cross-linking between the printed layers. The flexural strength and modulus of the 3D printed structures increased with increasing LG content to a mixing ratio of 0.5 and then leveled off at higher LG contents. The 0.25LG-NC structure (25.68 wt % NC solid content) shows a flexural strength of 98.23 ± 0.92 MPa, corresponding to a 171% increase compared to the pristine NC structure. Its modulus reaches 8.81 ± 0.26 GPa, increasing by 118% compared to that of the pristine NC structure. The 3D printed 0.5LG-NC structure shows a flexural strength of 102.93 ± 0.96

MPa and a flexural modulus of 9.05 ± 0.07 GPa. It shows similar mechanical properties to the 0.2SLG-NC structure except for strain-at-break, slightly reducing due to more LG contents. However, the 0.75SLG-NC structure shows a flexural strength of 85.98 ± 1.96 and a flexural modulus of 8.63 ± 1.01 GPa. The strain-at-break of all structures containing LG nanofillers decreased compared to that of the pristine NC structure. LG contains many nonpolar hydrocarbon and benzene groups and polar hydroxyl groups, which can improve hydrophobicity and compatibility with NC. Furthermore, LG is strongly cross-linked in plants via a covalent bond with NC. Therefore, the LG content in 3D printed LG-NC structures provides good compatibility, resulting in better interphase between the printed layers and better mechanical strength.

Broadly, the incorporation of fillers into a polymer matrix can yield enhancements in interfacial interactions and mechanical attributes, which are achieved by mitigating primary load-bearing responsibilities and the constraint of deformations arising from external stresses. Therefore, filler dispersibility and strong interfacial adhesion between the fillers and the polymeric matrix are critical to improving their mechanical properties. The mechanical properties of 3D printed NC structures mainly depend on the interactions between the constituents of NC paste, the aspect ratio of the fibers, and the dispersion of fillers within the NC paste. For adequate adhesion between the printed layers, the surface energy of the nanofillers should be as low or lower than the primary polymer (CNC/CNF) surface energy.³⁵ Different research studies have reported that the surface energy values for pristine NC are as high as 70 mJ/m^2 .³⁶ LG has a relatively lower surface energy of $53\text{--}56 \text{ mJ/m}^2$ ³⁷ than NC,³⁸ resulting in strong adhesion between the printed layers via more C–C and C–H bonds.

Compared to prior studies on high NC-content ($\sim 25 \text{ wt } \%$) 3D printed structures, the benefits shown in the current study using LG as a nanofiller are promising. Hausmann et al.³⁰ described a wet densification procedure after printing high-concentration NC structures in which the aqueous phase of the manufactured wet structures was exchanged with an organic liquid solution that serves as a weak solvent for the NC. After the densification process, the flexural strength and modulus of the structures were improved to 40 MPa and 7.9 GPa, respectively, which are significantly lower than our proposed results. According to Klar et al.,²⁹ the primary challenging issue is adhesive propensity between the printed layers at a high consistency of NC (25 wt %). The reported results demonstrated that the enzymatic treatment of NC is insufficient to improve the adhesion between layers, resulting in a low tensile strength of 17.6 MPa. Moreover, Latif et al.¹¹ utilized citric acid in concentrated NC structures to improve the adhesion between the printed layers to enhance shape fidelity and mechanical properties. However, the highest flexural strength and Young's modulus of the esterified NC structures (82.78 MPa and 6.97 GPa, respectively) are still lower than the current study results. The 3D printed 0.5LG-NC structures revealed the highest flexural strength of 102.93 ± 0.96 MPa and flexural modulus of 9.05 ± 0.07 GPa. Thus, this content is considered an optimum condition for the 3D printing of LG-blended NC.

3.4. Scanning Electron Microscopy. Figure 5a shows the cross-sectional morphology of the 0.5LG-NC scaffold structure. The scaffold structure showed a strong adhesion between the printed layers, resulting in a high structure shape

fidelity. Figure 5b shows a cross-sectional SEM image of the 0.5LG-NC structure after the flexural test. Figure 5c shows side-view images of the 0.5LG-NC structure reflecting strong adhesion without porosity. The printed lignocellulose layers showed a nonporous structure with a significant adhesion propensity in the horizontal and transverse directions. The significant mechanical strength of the optimized 0.5LG-NC structure is attributed to the strong adhesion between the printed layers, confirmed by the SEM (yellow circles show the adhesion between the 3D printed layers). The gaps/holes between the printed layers due to the high solid content can be seen in SEM images, which can be reduced by infusion of polymer resin. Hausmann et al.³⁰ infused acrylate/PUA oligomers after wet densification of 3D printed structures to reduce the gaps/holes between the printed layers. The uniformity in the printed layers confirms the excellent mixing of LG in NC without any agglomerations.

3.5. Shape Fidelity of 3D Printed Complex Structures.

The primary objective underlying the pursuit of shape fidelity and reproducibility using the optimized paste formulation resides in its facilitation of the design and fabrication of engineering structures. These structures hinge on the controlled shrinkage behavior exhibited by 3D printed LG-NC structures after the drying process, compelled by the evaporation of water. The shape fidelity and repeatability of the structures were evaluated by printing 16 box-shaped structures shown in Figure 6 with the optimized 0.5LG-NC paste and

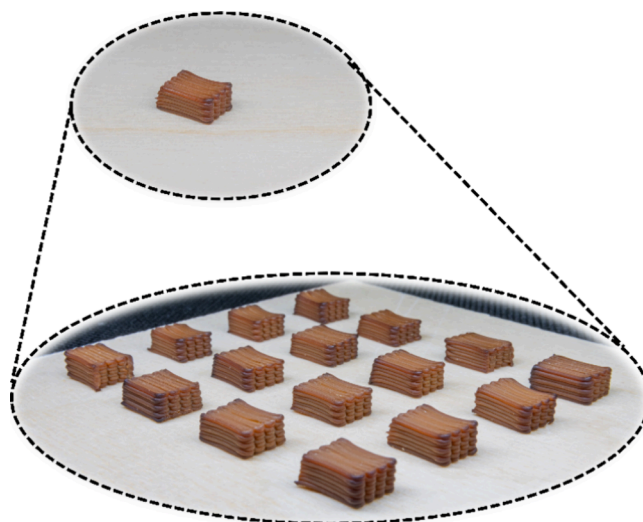


Figure 6. Lignocellulose 3D printed box-shaped structures were designed for shape fidelity.

drying under clean room and postcuring conditions. Table 3 shows the dimensions of the box-shaped structures after 3D printing, drying, and postcuring. The 0.5LG-NC structures

Table 3. Dimensions of 3D Printed Box-Shaped Structures

conditions	printed sample dimensions				
	length (mm)	width (mm)	height (mm)	volume (mL)	density (g/cm^3)
printed samples	12.08	12.08	9.31	1.36	
clean room	10.13 ± 0.16	7.67 ± 0.34	4.37 ± 0.13	0.34 ± 0.02	1.18
dried					
after postcuring at 140 °C	9.99 ± 0.17	7.45 ± 0.36	4.19 ± 0.16	0.31 ± 0.02	1.20

showed a significant volume shape fidelity and repeatability by a minor standard deviation of 0.021 before and after postcuring.

It is clear from Figure 6 that at a high solid concentration of NC, the LG plays an influential role as a cross-linker to improve the adhesion propensity between the layers during the drying stage. The samples showed 16.14, 36.50, and 53.06% shrinkages in length, width, and height before postcuring due to water evaporation, respectively. The observable shrinkage phenomenon within NC structures arises from water evaporation throughout the drying phases. However, the primary point is that the structures kept their original shapes even after drying, keeping a high content of NC (25.45 wt % solid content) without any adhesion or debonding issues, as reported in previous studies.^{29,30} The postcured structures at 140 °C for 30 min showed 1.38, 2.86, and 4.11% shrinkages in length, width, and height, respectively. The density of the postcured structures increased from 1.182 to 1.200 g/cm³ due to minor volumetric shrinkage. Previous studies reported debonding issues between the printed layers at high concentrations of NC, which resulted in poor shape fidelity compared to the original CAD design. However, LG as a nanofiller in NC resulted in strong adhesion between the layers, as confirmed by SEM images, which validated the high shape fidelity of the printed structures.

Furthermore, the optimized 0.5LG-NC paste was used to print complex structures, i.e., flower vases and biomedical scaffolds, as shown in Figure 7a,b. After drying under

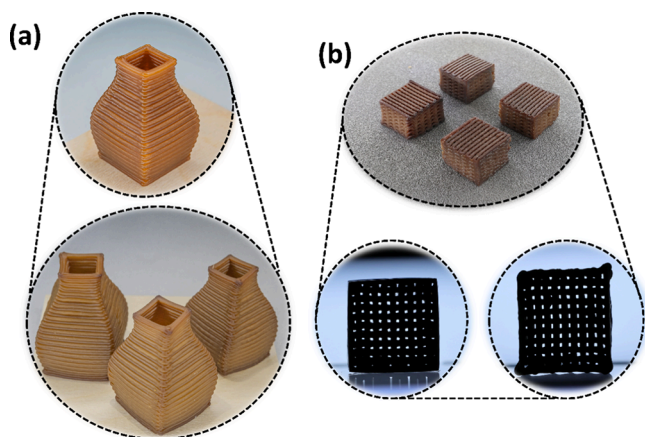


Figure 7. 3D printed LG-NC structures: (a) flower vase and (b) rigid scaffold structures.

optimized clean room conditions, the 3D printed flower vase structure and biomedical scaffold showed a substantial adhesion between the printed lignocellulose layers. Biopolymers such as NC have been demonstrated extensively as a replacement for synthetic polymers used in tissue repair due to their nontoxic nature.³⁹ The biopolymer-based scaffolds are mainly used to repair hard or soft tissues in tissue engineering.⁴⁰ Our results demonstrate an economical approach to printing a rigid 3D scaffold, as shown in Figure 7b, with pore-free microstructures with optimized 0.5LG-NC paste, which is a potential candidate for hard tissue engineering applications. Further studies are needed for its biomedical applications regarding cell viability, toxicity, antimicrobial activity, etc. Properly adjusting the NC concentration and cellular architecture of the printed scaffolds can open up many

possibilities for designing biocompatible cellulose-based structures for biomedical and functional applications.

4. CONCLUSIONS

The challenging issues, including repeatability, mechanical strength, and shape fidelity in 3D printed high-content (25.45 wt %) NC structures, were resolved effectively by incorporating LG as a nanofiller. A high solid content (25.95 wt %) lignocellulose (LG-NC) paste was prepared and extruded using a twin-screw extruder to 3D print, and the 3D printed structures were dried under clean room conditions. The 0.5LG-NC structure showed better mechanical properties (flexural strength = 101.57 ± 3.03 MPa; flexural modulus = 9.28 ± 0.46 GPa) than the pristine NC structure due to the improved adhesion between printed layers, indicating that the LG effectively increased the adhesion between the printed layers. Furthermore, the 3D printed box-shaped structures preserved the original CAD designs with small volume shrinkage after complete drying without adhesion issues, reflecting a high shape fidelity. Similarly, the low standard deviations of 0.020 (overall volume) indicate structures' high repeatability with the optimized paste (0.5LG-NC). The proposed facile approach to achieve high mechanical strength and shape fidelity in 3D printed high-content NC structures can be adapted for high-performance engineering and biomedical applications to manufacture high mechanical strength environment-friendly structures.

■ AUTHOR INFORMATION

Corresponding Author

Jaehwan Kim – Creative Research Center for Nanocellulose Future Composites, Department of Mechanical Engineering, Inha University, Incheon 22212, South Korea; orcid.org/0000-0002-6152-2924; Email: jaehwan@inha.ac.kr

Authors

Yangxiaoze Jiang – Creative Research Center for Nanocellulose Future Composites, Department of Mechanical Engineering, Inha University, Incheon 22212, South Korea; orcid.org/0000-0002-5200-9897

Muhammad Latif – Creative Research Center for Nanocellulose Future Composites, Department of Mechanical Engineering, Inha University, Incheon 22212, South Korea

Complete contact information is available at:

<https://pubs.acs.org/10.1021/acsomega.3c10101>

Author Contributions

Conceptualization: J.K. and Y.J.; data curation and experiments: Y.J. and M.L.; writing—original draft preparation: Y.J.; visualization: M.L.; writing—review and editing: J.K., M.L., and Y.J.; supervision: J.K. All authors have approved the final version of the manuscript.

Notes

The authors declare no competing financial interest.

■ ACKNOWLEDGMENTS

The National Research Foundation of Korea supported this research through the Creative Research Initiatives Program (NRF-2015R1A3A2066301).

REFERENCES

- (1) Levenhagen, N. P.; Dadmun, M. D. Reactive Processing in Extrusion-Based 3D Printing to Improve Isotropy and Mechanical Properties. *Macromolecules* **2019**, *52*, 6495–6501.
- (2) Sandmeier, M.; Paunović, N.; Conti, R.; Hofmann, L.; Wang, J.; Luo, Z.; Masania, K.; Wu, N.; Kleger, N.; Coulter, F. B.; Studart, A. R.; Grützmaier, H.; Leroux, J. C.; Bao, Y. Solvent-Free Three-Dimensional Printing of Biodegradable Elastomers Using Liquid Macrophotoinitiators. *Macromolecules* **2021**, *54*, 7830–7839.
- (3) Liu, Q.; Jain, T.; Peng, C.; Peng, F.; Narayanan, A.; Joy, A. Introduction of Hydrogen Bonds Improves the Shape Fidelity of Viscoelastic 3D Printed Scaffolds While Maintaining Their Low-Temperature Printability. *Macromolecules* **2020**, *53*, 3690–3699.
- (4) Serafin, A.; Culebras, M.; Oliveira, J. M.; Koffler, J.; Collins, M. N. 3D Printable Electroconductive Gelatin-Hyaluronic Acid Materials Containing Polypyrrole Nanoparticles for Electroactive Tissue Engineering. *Adv. Compos. Hybrid Mater.* **2023**, *6*, 109.
- (5) Galarreta-Rodriguez, I.; Lopez-Ortega, A.; Garayo, E.; Beato-López, J. J.; La Roca, P.; Sanchez-Alarcos, V.; Recarte, V.; Gómez-Polo, C.; Pérez-Landazábal, J. I. Magnetically Activated 3D Printable Polylactic Acid/Polycaprolactone/Magnetite Composites for Magnetic Induction Heating Generation. *Adv. Compos. Hybrid Mater.* **2023**, *6*, 102.
- (6) Jambhulkar, S.; Ravichandran, D.; Thippanna, V.; Patil, D.; Song, K. A Multimaterial 3D Printing-Assisted Micropatterning for Heat Dissipation Applications. *Adv. Compos. Hybrid Mater.* **2023**, *6*, 93.
- (7) Lu, C.; Deng, K.; Porter, A.; Fu, K. Top-down Digital Light Processing 3D Printing of Composite Structures Using Carbon Fiber Modified UV Curable Resin. *Adv. Compos. Hybrid Mater.* **2023**, *6*, 42.
- (8) Dai, L.; Cheng, T.; Duan, C.; Zhao, W.; Zhang, W.; Zou, X.; Aspler, J.; Ni, Y. 3D Printing Using Plant-Derived Cellulose and Its Derivatives: A Review. *Carbohydr. Polym.* **2019**, *203*, 71–86.
- (9) Auminate, C.; Soatthyanon, N.; Makmoon, T.; Potiyaraj, P. Polylactic Acid/Kenaf Cellulose Biocomposite Filaments for Melt Extrusion Based-3D Printing. *Cellulose* **2021**, *28*, 8509–8525.
- (10) Heggset, E. B.; Strand, B. L.; Sundby, K. W.; Simon, S.; Chinga-Carrasco, G.; Syverud, K. Viscoelastic Properties of Nanocellulose Based Inks for 3D Printing and Mechanical Properties of CNF/Alginate Biocomposite Gels. *Cellulose* **2019**, *26*, 581–595.
- (11) Latif, M.; Jiang, Y.; Kumar, B.; Song, J. M.; Cho, H. C.; Kim, J. High Content Nanocellulose 3D-Printed and Esterified Structures with Strong Interfacial Adhesion, High Mechanical Properties, and Shape Fidelity. *Adv. Mater. Interfaces* **2022**, *9*, 2200280.
- (12) Latif, M.; Jiang, Y.; Song, J.; Kim, J. Additively-Manufactured High-Concentration Nanocellulose Composites: Structure and Mechanical Properties. *Polymers (Basel)* **2023**, *15*, 669.
- (13) Latif, M.; Jiang, Y.; Kim, J. 3D Printing of Concentrated Nanocellulose Material: The Critical Role of Substrates on the Shape Fidelity and Mechanical Properties. *Carbohydr. Polym.* **2023**, *320*, No. 121197.
- (14) Latif, M.; Jiang, Y.; Kumar, B.; Cho, H. C.; Song, J. M.; Kim, J. Three-Dimensional Printing of Highly Crosslinked and Concentrated Nanocellulose for Environmentally Friendly Structural Applications. *ACS Appl. Nano Mater.* **2022**, *5*, 5680–5687.
- (15) Wang, J.; Zhang, D.; Chu, F. Wood-Derived Functional Polymeric Materials. *Adv. Mater.* **2021**, *33*, 2001135.
- (16) Ponnusamy, V. K.; Nguyen, D. D.; Dharmaraja, J.; Shobana, S.; Banu, J. R.; Saratale, R. G.; Chang, S. W.; Kumar, G. A Review on Lignin Structure, Pretreatments, Fermentation Reactions and Biorefinery Potential. *Biores. Technol.* **2019**, *271*, 462–472.
- (17) Habibi, Y.; Lucia, L. A.; Rojas, O. J. Cellulose Nanocrystals: Chemistry, Self-Assembly, and Applications. *Chem. Rev.* **2010**, *110*, 3479–3500.
- (18) Kim, J. H.; Shim, B. S.; Kim, H. S.; Lee, Y. J.; Min, S. K.; Jang, D.; Abas, Z.; Kim, J. Review of Nanocellulose for Sustainable Future Materials. *Int. J. Precis. Eng. Manufact. - Green Technol.* **2015**, *2*, 197–213.
- (19) Kim, J.; Yun, S.; Ounaies, Z. Discovery of Cellulose as a Smart Material. *Macromolecules* **2006**, *39*, 4202–4206.
- (20) Xu, W.; Molino, B. Z.; Cheng, F.; Molino, P. J.; Yue, Z.; Su, D.; Wang, X.; Willför, S.; Xu, C.; Wallace, G. G. On Low-Concentration Inks Formulated by Nanocellulose Assisted with Gelatin Methacrylate (GelMA) for 3D Printing toward Wound Healing Application. *ACS Appl. Mater. Interfaces* **2019**, *11*, 8838–8848.
- (21) Markstedt, K.; Mantas, A.; Tournier, I.; Martínez Ávila, H.; Hägg, D.; Gatenholm, P. 3D Bioprinting Human Chondrocytes with Nanocellulose-Alginate Bioink for Cartilage Tissue Engineering Applications. *Biomacromolecules* **2015**, *16*, 1489–1496.
- (22) Leppiniemi, J.; Lahtinen, P.; Paajanen, A.; Mahlberg, R.; Metsä-Kortelainen, S.; Pinomaa, T.; Pajari, H.; Vikholm-Lundin, I.; Pursula, P.; Hytönen, V. P. 3D-Printable Bioactivated Nanocellulose-Alginate Hydrogels. *ACS Appl. Mater. Interfaces* **2017**, *9*, 21959–21970.
- (23) Martínez Ávila, H.; Schwarz, S.; Rotter, N.; Gatenholm, P. 3D Bioprinting of Human Chondrocyte-Laden Nanocellulose Hydrogels for Patient-Specific Auricular Cartilage Regeneration. *Bioprinting* **2016**, *1–2*, 22–35.
- (24) Fourmann, O.; Hausmann, M. K.; Neels, A.; Schubert, M.; Nyström, G.; Zimmermann, T.; Siqueira, G. 3D printing of shape-morphing and antibacterial anisotropic nanocellulose hydrogels. *Carbohydr. Polym.* **2021**, *259*, 1–11.
- (25) Wang, Q.; Sun, J.; Yao, Q.; Ji, C.; Liu, J.; Zhu, Q. 3D Printing with Cellulose Materials. *Cellulose* **2018**, *25*, 4275–4301.
- (26) Müller, L. A. E.; Zimmermann, T.; Nyström, G.; Burgert, I.; Siqueira, G. Mechanical Properties Tailoring of 3D Printed Photo-responsive Nanocellulose Composites. *Adv. Funct. Mater.* **2020**, *30*, 2002914.
- (27) Håkansson, K. M. O.; Henriksson, I. C.; de la Peña Vázquez, C.; Kuzmenko, V.; Markstedt, K.; Enoksson, P.; Gatenholm, P. Solidification of 3D Printed Nanofibril Hydrogels into Functional 3D Cellulose Structures. *Adv. Mater. Technol.* **2016**, *1*, 1600096.
- (28) Rees, A.; Powell, L. C.; Chinga-Carrasco, G.; Gethin, D. T.; Syverud, K.; Hill, K. E.; Thomas, D. W. 3D Bioprinting of Carboxymethylated-Periodate Oxidized Nanocellulose Constructs for Wound Dressing Applications. *Biomed. Res. Int.* **2015**, *2015*, 925757.
- (29) Klar, V.; Pere, J.; Turpeinen, T.; Kärki, P.; Orelma, H.; Kuosmanen, P. Shape Fidelity and Structure of 3D Printed High Consistency Nanocellulose. *Sci. Rep.* **2019**, *9*, 3822.
- (30) Hausmann, M. K.; Siqueira, G.; Libanori, R.; Kokkinis, D.; Neels, A.; Zimmermann, T.; Studart, A. R. Complex-Shaped Cellulose Composites Made by Wet Densification of 3D Printed Scaffolds. *Adv. Funct. Mater.* **2020**, *30*, 190427.
- (31) Huan, S.; Ajdary, R.; Bai, L.; Klar, V.; Rojas, O. J. Low Solids Emulsion Gels Based on Nanocellulose for 3D-Printing. *Biomacromolecules* **2019**, *20*, 635–644.
- (32) Makarem, M.; Lee, C. M.; Kafle, K.; Huang, S.; Chae, I.; Yang, H.; Kubicki, J. D.; Kim, S. H. Probing Cellulose Structures with Vibrational Spectroscopy. *Cellulose* **2019**, *26*, 35–79.
- (33) Soni, B.; Hassan, E. B.; Mahmood, B. Chemical Isolation and Characterization of Different Cellulose Nanofibers from Cotton Stalks. *Carbohydr. Polym.* **2015**, *134*, 581–589.
- (34) Alassod, A.; Islam, S. R.; Farooq, A.; Xu, G. Fabrication of Polypropylene/Lignin Blend Sponges via Thermally Induced Phase Separation for the Removal of Oil from Contaminated Water. *SN Appl. Sci.* **2020**, *2*, 1569.
- (35) Khoshkava, V.; Kamal, M. R. Effect of Surface Energy on Dispersion and Mechanical Properties of Polymer/Nanocrystalline Cellulose Nanocomposites. *Biomacromolecules* **2013**, *14*, 3155–3163.
- (36) Hosseinmardi, A.; Annamalai, P. K.; Martine, B.; Pennells, J.; Martin, D. J.; Amiralian, N. Facile Tuning of the Surface Energy of Cellulose Nanofibers for Nanocomposite Reinforcement. *ACS Omega* **2018**, *3*, 15933–15942.
- (37) Notley, M. S.; Norgren, M. Surface Energy and Wettability of Spin-Coated Thin Films of Lignin Isolated from Wood. *Langmuir* **2010**, *26*, 5484–5490.
- (38) Österberg, M.; Sipponen, M. H.; Mattos, B. D.; Rojas, O. J. Spherical Lignin Particles: A Review on Their Sustainability and Applications. *Green Chem.* **2020**, *22*, 2712–2733.

(39) Xue, Y.; Mou, Z.; Xiao, H. Nanocellulose as a Sustainable Biomass Material: Structure, Properties, Present Status and Future Prospects in Biomedical Applications. *Nanoscale* **2017**, *9*, 14758–14781.

(40) Iravani, S.; Varma, R. S. Greener Synthesis of Lignin Nanoparticles and Their Applications. *Green Chem.* **2020**, *22*, 612–636.